From moduli scaling to breakdown scaling: A moment-spectrum analysis

Y. S. Li and P. M. Duxbury
Physics and Astronomy Department and Center for Fundamental Materials Research, Michigan State University, East Lansing, Michigan 48824-1116
(Received 20 March 1989)

Conductivity and elastic moduli are related to the second moment of the appropriate field distribution in a disordered material. We argue that breakdown is related to the very high moments of this local-field distribution, and the moment spectrum thus quantifies the crossover between these two very different classes of properties. We first analyze the moment spectrum, and hence the moduli to breakdown crossover, for an isolated cracklike flaw in electrical, dielectric, and mechanical problems. A result central to this analysis is the form of the electric field or stress distribution due to such a crack. The Appendix collects these scaling forms for a cracklike elliptical (or ellipsoidal) void in electrical and mechanical problems and for a long, thin metallic inclusion in a dielectric and is a major component of the paper. When a distribution of flaws is present in a material, the moment value at which crossover to extreme scaling occurs is determined by the asymptotic form of the tail of the local load distribution. We discuss the location of this crossover for exponential, algebraic, and multifractal tails. Finally, we discuss the ability of the moment spectrum of the local load distribution to provide nondestructive tests of the presence of large and/or sharp cracklike flaws in a material. We show that for moment values $m > 4$ it is possible to detect the presence of a sharp crack in electrical and mechanical problems. In three-dimensional dielectrics containing a sharp metal inclusion, it is shown that such detection is possible for $m > 3$.

I. INTRODUCTION

If a constant external electric field or stress is applied to an inhomogeneous material, the local stress or electric field shows strong spatial fluctuations.[1,2] The size of these local load fluctuations is quantified by a distribution function we call the local load distribution $L(x)$. This distribution function has been intensively studied recently in the context of the voltage distribution at the percolation point, where it has been labeled multifractal.[1] In this paper, we show that the moment spectrum induced by a random environment provides a useful concept in which to understand the differences between the scaling behavior characteristic of transport[3] and elastic[4] moduli and the very different scaling behavior characteristic of breakdown properties.[5]

It is known that the effective conductivity of an inhomogeneous material is related to the second moment of $L(x)$,[3] while the resistive noise is related to the fourth moment of this distribution.[6,7] In a similar way, properties such as elastic constant and thermal conductivity are related to the second moment of the appropriate local load distributions. By contrast, fracture strength, dielectric strength and other *breakdown properties* are initiated in regions where the local load is largest.[5] It is intuitively plausible, and in this paper we give quantitative evidence that, these load *hotspots* are related to the very high moments of the local load distribution. A study of the full moment spectrum thus allows us to understand in detail the crossover from low-moment scaling (transport properties, etc.) to high-moment scaling (hotspots and breakdown properties).

To study this crossover, we first focus attention on isolated cracklike flaws that most enhance local fields. The low-moment–to–high-moment crossover of systems containing such isolated cracks is discussed in Sec. II. To carry out the analysis, we need simple scaling forms for the local stress or electric field distributions near isolated cracks. These forms are derived in the Appendix, and are summarized in Eqs. (15) and (22) of the main text.

When a distribution of flaws is present in a material, it is not possible to find the detailed form of the stress or electric field distribution. Despite this, we argue in Sec. III that it is possible to estimate the point at which the crossover from low moment to extreme scaling occurs, by studying the form of the tail of the local load distribution. This analysis is carried out for systems with exponential, algebraic, and multifractal tails in $L(x)$. A numerical illustration of these arguments is provided by calculating the moment spectrum as a function of dilution for two-dimensional random resistor networks. These results are displayed in Fig. 3.

In addition to a summary of the main conclusions drawn in Secs. II and III, Sec. IV contains a discussion of the ability of various moments of the local load distribution to detect the presence of a large and/or sharp cracklike flaw in a material. This is an issue of central importance in nondestructive testing of materials and structures.

II. MOMENT SCALING DUE TO AN ISOLATED CRACKLIKE FLAW

Consider an isolated crack of length, a, and with a curvature at the crack tip, κ, in an otherwise, homogeneous

system with large volume $V=L^d$ ($a \ll L$). It is known that such an isolated crack (which is modeled as a cracklike void) makes negligible contribution to the overall conductivity, Σ_{eff}, i.e., that

$$\Sigma_{\text{eff}}/\Sigma_0 \sim 1-O(V_{\text{inc}}/V) , \tag{1}$$

where Σ_0 is the background conductivity and V_{inc} is the volume of the inclusion. By contrast, such an isolated crack drastically reduces the electrical and mechanical strength of the system, as near the crack tip, strong load enhancements occur, and for the electrical case one finds,

$$E_{\text{tip}}/E_0 \sim (a/2\kappa)^{1/2} \quad (\text{for } a \gg 1) , \tag{2}$$

which leads to an electrical strength of order

$$E_b(a)/E_b(0) \sim E_0/E_{\text{tip}} \sim (2\kappa/a)^{1/2} \quad (\text{for } a \gg 1) . \tag{3}$$

$E_b(a)$ is the electrical strength of the sample with a flaw in it, $E_b(0)$ is the electrical strength of the material with no flaws, and the electric field is applied perpendicular to the crack. The essential difference between the scaling forms (1) and (3) is that a crack of size, a, has very little effect on conductivity until $a \sim L$, while electrical strength reduces as the square root of, a, for all $1 \ll a \ll L$.

A similar square-root reduction in mechanical strength occurs in systems containing cracks, as can be seen from the (plane stress) Griffith formula[8] $\sigma_b=(2\gamma_0 e_0/\pi a)^{1/2}$, where γ_0 is the energy needed to create new crack surfaces, while e_0 is the elastic modulus of the background. If one approaches the mechanical problem from a stress analysis viewpoint, a similar expression to (3) holds for mechanical strength with E_b and E_0 replaced by stresses.[8] In this paper, we use stress and electric field intensity formalisms, as they provide a framework in which to better understand the crossover from moduli scaling to breakdown scaling.

To demonstrate that the moment spectrum of the local load distribution contains Eqs. (1) and (2) as limiting cases, note that the maximum electric field occurring in a system may be written,

$$E_{\max} \sim \langle E^m \rangle^{1/m}_{m\to\infty} , \tag{4a}$$

so that

$$E_b \text{ (flawed system)}/E_b(0) \sim \langle E_0 \rangle / \langle E^m \rangle^{1/m} \quad \text{as } m \to \infty . \tag{4b}$$

For the case of insulating inclusions, it can be seen that the effective conductivity is related to the second moment of the electric field distribution by noting that the power P

$$P = VE_0^2\Sigma_{\text{eff}} = \int E^2\Sigma(\bar{r})d\bar{r} = \Sigma_0\langle E^2\rangle V , \tag{5}$$

so that

$$\Sigma_{\text{eff}}/\Sigma_0 = \langle E_0^2\rangle / \langle E^2\rangle . \tag{6}$$

Comparing Eqs. (4b) and (6), it is seen that study of the function

$$R_m = \langle E_0\rangle / \langle E^m\rangle^{1/m} \tag{7}$$

provides a simple quantity that typifies the crossover from low-moment to extreme moment scaling as a function of m. For a system containing an isolated crack, this quantity shows a crossover from $O(1/V)$ corrections when m is small to the typical breakdown scaling of Eq. (3) when m becomes large. We now study this crossover analytically for electrical, mechanical, and dielectric systems containing an isolated crack.

Consider an isolated cracklike elliptical void in the geometry shown in Fig. 1. In elliptic coordinates, ξ, η,

$$x = c\cosh\xi\cos\eta, \quad z = c\sinh\xi\sin\eta \tag{8}$$

with the ellipse equation being

$$x^2/a^2 + z^2/b^2 = 1 \tag{9}$$

and

$$c^2 = a^2 - b^2 ,$$

and the electric field applied in the z direction has amplitude E_0 far from the ellipse. Solving Laplace's equation in elliptical coordinates yields the electric potentials,

$$\phi_{\text{in}} = -A\ c\sinh\xi\sin\eta , \tag{10a}$$

$$\phi_{\text{out}} = -E_0 c\sinh\xi\sin\eta + Be^{-\xi}\sin\eta , \tag{10b}$$

with

$$A = E_0(a+b)/b$$

and (10c)

$$B = -E_0 a(a+b)/c .$$

The electric fields are then given by

$$E_\xi = -(1/\tau)\partial\phi/\partial\xi$$

and (11)

$$E_\phi = -(1/\tau)\partial\phi/\partial\eta ,$$

where

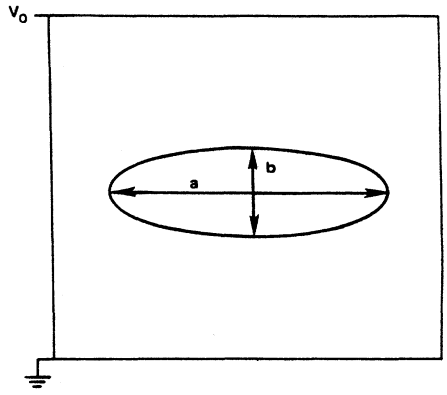

FIG. 1. The geometry of the two-dimensional ellipse problem.

$$\tau = c(\sinh^2\xi + \sin^2\eta)^{1/2} . \tag{12}$$

The full expression for the electric field moments is given by

$$\langle E^m \rangle = (1/V)\int_V (E_\xi^2 + E_\eta^2)^{m/2} dV . \tag{13}$$

It is known that the second moment ($m=2$) and inclusion energy scale as

$$\langle E^2 \rangle / \langle E_0^2 \rangle \sim 1 + O(1/V) , \tag{14}$$

the corrections to the conductivity due to the isolated crack are related to the second moment [see Eq. (6)], and this implies Eq. (1) for a single crack. We have not been able to analytically evaluate Eq. (13) for any $m > 2$, but the important scaling behavior may be found by noting that the electric field as a function of radial distance parallel to the major axis of the ellipse behaves as shown in Fig. 2(a). The important scaling behavior that occurs in this figure is summarized mathematically by (see the Appendix)

$$E_z(r)/E_0 \sim \begin{cases} 1 + \alpha_{2e}/r^d & \text{for } r \gg a , \quad (15a) \\ c_{1e} + c_{2e}(a/2r)^{1/2} & \text{for } \kappa < r < a , \quad (15b) \\ k_{1e} + k_{2e}(a/2\kappa)^{1/2} & \text{for } r < \kappa , \quad (15c) \end{cases}$$

where α_{2e} is a dipole moment for the two-dimensional problem of a crack in a resistive background, κ is the crack tip curvature ($=b^2/a$) for an ellipse, and c_{1e}, c_{2e}, k_{1e}, and k_{2e} are constants for the two-dimensional (2D) electrical problem. In fact, the scaling behavior of Eq. (15) is highly universal, and applies (with different α, c, and k) to ellipse, ellipsoidal, and slitlike cracks in 2D and 3D linear elastic (plain stress) and electric problems (see the Appendix). This is illustrated for the 3D elastic problem in Fig. 2(b) where the z-direction stress is plotted as a function of radial distance from the tip of an oblate ellipsoidal void (in the x-y plane). Again, the near-field square-root behavior crosses over to a far-field dipole form, in agreement with Eq. (15). As seen from Eq. (15b), an important singular behavior occurs near the crack tip, and the angular dependence (to x axis) of this singular behavior is

$$\begin{aligned} E_r(r,\theta) &\sim E_0(a/2r)^{1/2}\sin(\theta/2) , \\ E_\theta(r,\theta) &\sim E_0(a/2r)^{1/2}\cos(\theta/2) , \end{aligned} \tag{16}$$

for θ small. This more general form does not, however, change the moment scaling behavior derived below, and henceforth we use Eq. (15) in our scaling analysis. The most important physical observation is that as the moment value is increased, the regions (15b) and (15c) increase their contribution to the integral (13). This is explicitly seen by subdividing and approximating the integral (13) as shown below:

$$\begin{aligned} V\langle [E(r)/E_0]^m \rangle \sim & \int_{r>a} r\,dr(1+\alpha_{2e}/r^d)^m \\ & + \int_{\kappa<r<a} r\,dr[c_{1e}+c_{2e}(a/2r)^{1/2}]^m \\ & + \int_{r<\kappa} r\,dr[k_{1e}+k_{2e}(a/2\kappa)^{1/2}]^m . \end{aligned} \tag{17}$$

Keeping the most singular terms in each integral, we find

$$\langle [E(r)/E_0]^m \rangle \sim 1 + mO(V_{\rm inc}/V) + (a/2\kappa)^{m/2}\kappa^2/V , \tag{18}$$

where $V_{\rm inc}$ is the volume of the inclusion. The $O(V_{\rm inc}/V)$ term is estimated by considering the leading term in the first integral, and including the correct angular terms. This is necessary, as this term is a dipole integral, in which care must be taken to ensure that all terms are included, and that boundary terms do not produce unphysical results. The result is a term of order the inclusion energy, which leads directly to the result quoted.

From Eq. (18), we can see that R_m [see Eq. (7)] has the following scaling forms:

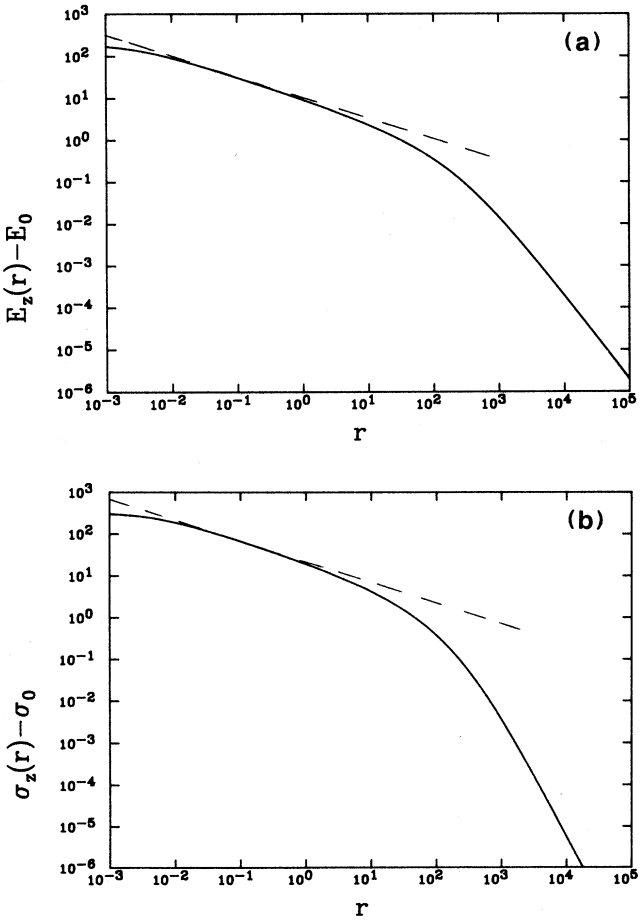

FIG. 2. (a) The ($z=0$) electric field, $E_z(r)$, as a function of distance from the tip of an ellipse ($a=200$, $b=1$). The mathematical form of the scaling behavior in $E_z(r)$ is given in Eq. (15) of the text. (b) The $z=0$ stress field, $\sigma_z(r)$, as a function of r for an oblate ellipsoid ($a=200$, $b=1$) in an elastic background. The dashed line has slope $-\frac{1}{2}$.

$$R_m \sim \begin{cases} 1-O(V_{\rm inc}/V), & m \ll m_c \ , \\ (2\kappa/a)^{1/2}, & m \gg m_c \ , \end{cases} \tag{19}$$

where m_c is found from

$$(a/2\kappa)^{m/2}\kappa^2/V \sim 1 \tag{20}$$

or

$$m_c \sim 2\ln(V/\kappa^2)/\ln(a/2\kappa) \ . \tag{21}$$

Due to the universality of Eq. (15), this result straightforwardly generalizes to three-dimensional electric problems and to elastic problems in two and three dimensions.

There is also a great deal of similarity between the problem of an insulating crack in an conducting background and the problem of a conducting crack in an insulating background. The former problem has been discussed as the simplest example of an electrical breakdown problem,[5] while the latter is the simplest starting point for understanding defect-induced dielectric breakdown.[5,9] It is well known that in two dimensions, the electric field enhancement at the tip of a metal ellipse oriented parallel to the applied electric field in an insulating background, is the same as that at the tip of a void inclusion oriented perpendicular to the applied field and in a conducting background (see the Appendix). The asymptotic form (15) then applies equally well to the dielectric problem in two dimensions, and hence that Eqs. (17)–(21) express the moment scaling appropriate to that problem. The dielectric problem is different in three dimensions, however, as there the most important cracklike defect is a fingerlike inclusion,[5,9] which induces the following electric field behavior near its tip [see Eqs. (A28)–(A33) of the Appendix]:

$$E_z(r)/E_0 \sim \begin{cases} 1+\alpha_{3d}/r^3 \ \text{ for } \ r>a \ , \\ \ln(r/2a)+a/2r \ \text{ for } \ \kappa<r<a \ , \\ 1+(a/b)^2/\ln(2a/b) \ \text{ for } \ r<\kappa \ , \end{cases} \tag{22}$$

in this case the integration over the region near the crack tip leads to

$$\begin{aligned} V\langle [E(r)/E_0]^m\rangle \sim & \int_a^L r^2(1+\alpha_{3d}/r^3)^m dr \\ & + \int_\kappa^a r^2 dr[\ln(r/2a)+a/2r]^m \\ & + \kappa^3[1+(a/b)^2/\ln(a/b)]^m \ , \end{aligned} \tag{23}$$

so that

$$\langle [E(r)/E_0]^m\rangle \sim 1+mO(V_{\rm inc}/V)+(a/2\kappa)^m\kappa^3/V \ . \tag{24}$$

The moment value at which crossover between low-moment scaling and extreme scaling occurs is then given by

$$m_c \sim \ln(V/\kappa^3)/\ln(a/2\kappa) \ . \tag{25}$$

For extremely sharp cracks ($\kappa \to 0$), it is seen from Eqs. (18) and (24) that if κ becomes sufficiently small, a singular behavior can occur for low-moment values. For the problems described by Eq. (18) this moment value is

$$m_{c1}=4 \ , \tag{26}$$

while for the 3D dielectric problem [see Eq. (24)],

$$m_{c1}=3 \ . \tag{27}$$

For $m > m_{c1}$, moments are affected by extremely sharp cracks, and in fact these moments are singular as $\kappa \to 0$ (see also Ref. 7).

III. SYSTEMS WITH FLAW DISTRIBUTIONS

In this section, we consider systems with a distribution of voids. These voids are randomly distributed and may have any shape. When such a distribution of flaws is present in a material, a distribution of local loads is induced. The point at which extreme scaling sets in, is determined by the form of the *tail of the local load distribution* $L(x)$. In this section we consider exponential, algebraic, and multifractal load distribution tails. A specific illustration of our results is provided by numerical studies on random resistor networks.

A. Exponential tails in $L(x)$—$p > p_c$ random resistor networks

When the dilution, $f=1-p$, is small, the distribution of bond currents (and hence voltages) in the 2D $L\times L$ random resistor network is known to be exponential.[2] In this case, the largest current in a system of size L^d is of order $I_{\rm max} \sim \ln L$, and for a fixed applied current of L amps, the high moments of $L(I)$ are then approximated by

$$\langle I^m\rangle \sim A\int^{I_{\rm max}} I^m \exp(-AI)dI \ . \tag{28}$$

This is true as long as $m/A \gg 1$, and $A \sim -\ln(1-p)$ for p small. As p approaches p_c, A becomes small, and a multifractal bond current distribution must be considered.[1] The integrand in Eq. (28) has a maximum at $I_{\rm peak} \sim m/A$, after which it decays exponentially. If this peak lies far above the upper limit of the integral in Eq. (28), the algebraic term dominates, and the integral is approximated by

$$\langle I^m\rangle \sim (\ln L)^{m+1}/(m+1) \ \text{ for } \ m > m_c \sim \ln L \tag{29}$$

so that

$$\langle I^m\rangle^{1/m} \sim \ln L \sim I_{\rm max} \ . \tag{30}$$

Thus, for $m > m_c \sim \ln L$, moments drawn from an exponential local load distribution exhibit extreme scaling. For $m < m_c$ the full integral in (28) must be calculated, and in this regime the systems exhibit low-moment scaling. To illustrate the crossover from low-moment to high-moment scaling numerically, we present in Fig. 3 these moments calculated for 100×100 random resistor networks for a range of values of p. In these calculations we find $\langle I_0\rangle/\langle I^m\rangle^{1/m}$ for fixed external supplied current as a function of p. As in the single crack case, $m \to \infty$ yields a crossover to breakdown scaling, while low moments are nonsingular near the pure limit, as is the conductivity. A plot of these moments as a function of system size is shown in Fig. 4, where it is seen that low mo-

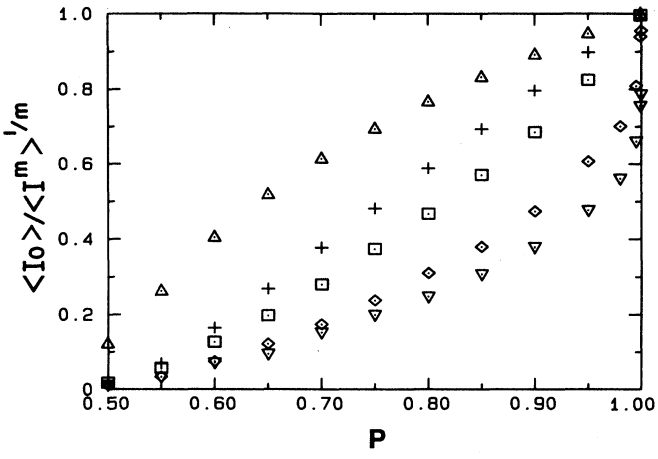

FIG. 3. Moment scaling as a function of dilution for 100×100 square lattice random resistor networks. $\langle I_0\rangle/\langle I^m\rangle^{1/m}$ is plotted on the vertical axis for ($\triangle$), $m=2$; ($\square$), $m=12$; ($\diamond$), $m=30$; (∇), I_b. For comparison the conductance is also plotted ($+$).

ments saturate at a finite value for large system sizes, while extreme moments continue to decrease logarithmically as a function of system size (this is the characteristic "size effect" of breakdown in random media[5]). Since $m_c\sim\ln L$, we find that each moment has a critical length associated with it, and that this critical length is given by $L_c\sim\exp(m)$. For $L>L_c(m)$, the moments saturate, while for $L<L_c(m)$, the moments show the $1/\ln L$ size effect characteristic of breakdown. In this sense, the breakdown limit is a critical point in moment space at which $L_c\to\infty$ exponentially.

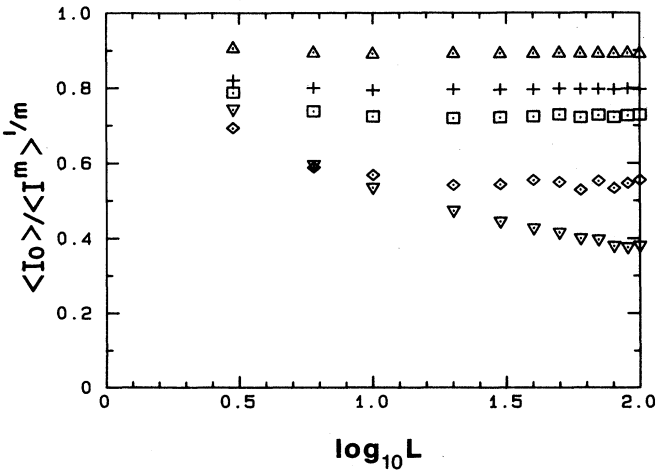

FIG. 4. $\langle I_0\rangle/\langle I^m\rangle^{1/m}$ as a function of system size for $p=0.90$ random resistor networks, for ($\triangle$), $m=2$; ($\square$), $m=10$; ($\diamond$), $m=20$; (∇), I_b. For comparison the conductance is also plotted ($+$).

B. Algebraic tails in $L(x)$

Consider a bond current distribution which is algebraically decaying in I and depends on a single exponent s. The current moments are then given by

$$\langle I^m\rangle\sim\int^{I_{\max}} I^{m-s}dI\ . \tag{31}$$

$I_{\max}$ is found from

$$I_{\max}^{-s}L\sim1\ ,$$

which implies

$$I_{\max}\sim L^{1/s}\ . \tag{32}$$

Evaluating the integral gives

$$\langle I^m\rangle\sim(L^{(m-s-1)/s}-1)/(m-s+1)\ . \tag{33}$$

For $m>s-1$, the first term in the parentheses dominates, and

$$\langle I^m\rangle\sim L^{x(m)/\nu}\ \text{ for } m>s-1\ , \tag{34}$$

where

$$x(m)=(m-s+1)\nu/s\ . \tag{35}$$

Here ν is the percolation correlation length exponent and is included in the definition of $x(m)$ for comparison with systems having a multifractal local load distribution (e.g., the percolation problem at p_c). From (34), we see that

$$\langle I^m\rangle^{1/m}\sim I_{\max}\sim L^{1/s} \tag{36}$$

provided $m\gg s-1$. That is, the bigger s is, the more slowly the crossover to extreme scaling occurs. As $s\to\infty$ the distribution becomes exponential, and $m_c\sim\ln L$ applies.

C. Multifractal $L(x)$

In this case, it is known that a moment scaling like that of Eq. (34) occurs, but that $x(m)$ is nonlinear in m [we note in passing that a plot of (33) also looks nonlinear in m]. However, for large enough m, the multifractal spectrum does become linear in m, and once this has occurred, the moment scaling is strongly affected by large currents. However, breakdown scaling does not become dominant until the condition $m\gg s$ prevails. In the multifractal case, s is the exponent one would get if the asymptotic linear behavior in the multifractal spectrum were extrapolated back to the origin. For the percolation problem it is seen from the data of Ref. 1 (Fig. 6) that $s\sim4$, so that extreme scaling and low-moment scaling become identical for moments in the part of the multifractal spectrum that is both linear and satisfies $m\gg4$.

IV. DISCUSSION AND CONCLUSIONS

We have shown that the moment spectrum occurring in a random system shows a crossover from low-moment scaling indicative of transport or elastic moduli, to extreme moment scaling indicative of breakdown scaling [see, e.g., Eqs. (18) and (19) and Fig. 3]. It was found that for $m\gg m_c$, the moments exhibited extreme scaling,

while for $m \ll m_c$, the scaling behavior is more characteristic of low-moment scaling [see Eqs. (20) and (21)]. This crossover is illustrated for random resistor networks in Figs. 3 and 4. When the disorder is stronger, so that algebraic or multifractal tails are induced in the local load distribution, the crossover to extreme scaling depends on the exponents characteristic of the tail of $L(x)$. In particular, it is evident that the crossover to extreme scaling occurs more quickly the longer the tail of the local load distribution becomes [see, e.g., Eq. (35) and the discussion following it].

For an isolated crack, although the crossover to extreme scaling does not occur until m_c as given by Eq. (21), another question of academic as well as practical interest (for nondestructive testing) is to determine the moment values at which crack tip effects first become experimentally observable. It is seen from Eqs. (17) and (18) and the discussion following these equations, that for electrical and mechanical problems, the effects of crack size and tip curvature become important for $m > 4$. In the two-dimensional dielectric problem, $m > 4$ is again required before crack effects become important. However, it is seen from Eq. (24) that for $m > 3$ the three-dimensional dielectric problem shows strong crack tip effects. In all of these cases, although measurements will evidence the presence of a crack, the measured signal is reduced by inverse-volume factors. Thus, although this sort of measurement is of academic interest, it is probably not a robust measure of the presence of cracks, as would be required for practical applications of nondestructive testing.[7]

From the foregoing discussion it is evident that methods for measuring the full moment spectrum of a material under load is of great practical as well as academic interest. Unfortunately, currently there is no experimental method for measuring other than the second moment (moduli), the fourth moment (noise, damping), and the infinite moment (breakdown properties).

ACKNOWLEDGMENTS

We thank the Composite Materials and Structures Center at Michigan State University for financial support.

APPENDIX

In this appendix, we outline the derivations of the central asymptotic forms given in Eqs. (15) and (22) of the text. These results are derived from existing solutions to ellipse and ellipsoidal inclusions in homogeneous backgrounds. These problems are classical and heavily studied, but to our knowledge this is the first time that the important scaling behaviors for both electrical and mechanical problems have been collected together and compared.

In all cases we consider an external electric field or tensile stress applied along the z direction. We also restrict our attention to the most severe flaws, namely, ellipses and oblate ellipsoid voids with their long axis perpendicular to the direction of applied load in the electrical and elastic cases, and ellipse and prolate ellipsoid perfect conductors with their long axis parallel to the direction of applied electric field in the case of dielectric problems. These ellipses and ellipsoids are characterized by one or two long axes, a, and one or two short axes, b, and we consider a/b large to simulate the most severe flaws.

1. Electrical problems

a. 2D insulating void in a conducting background

The solution for the electric potential is given in Eq. (10) of the text. The electric fields are then calculated using Eq. (11). Setting $\eta=0$, yields for the electric field in the z direction as a function of distance from the ellipse tip (on the $z=0$ line):

$$E_z(\xi)=E_0[1+\cosh\xi_0 \exp(\xi_0-\xi)/\sinh\xi] , \tag{A1}$$

where

$$\cosh\xi_0=a/c$$

and (A2)

$$\sinh\xi_0=b/c$$

with a, b, c, defined as in Eqs. (8) and (9) of the text. The electric field at the defect tip is then

$$E_{\rm tip}=E_0(1+a/b)=E_0[1+2^{1/2}(a/2\kappa)^{1/2}] \tag{A3}$$

with $\kappa=b^2/a$. Equation (A1) can be written in terms of r, the distance from the defect tip,

$$E_z(r)=E_0\left[1+\frac{a(a+b)[(a+r)-(2ar+r^2+b^2)^{1/2}]}{c^2(r^2+2ar+b^2)^{1/2}}\right] . \tag{A4}$$

A plot of Eq. (A4) is given in Fig. 2(a). When r is large, $E_z(r)$ asymptotes to a dipole form,

$$E_z(r)=E_0(1+\alpha_{2e}/r^2) \tag{A5}$$

with the electric dipole moment

$$\alpha_{2e}=a(a+b)/2 . \tag{A6}$$

Since the inclusion is sharp, the electric field becomes large near the defect tip [as seen in Eq. (A3)], the nature of this divergence is found from a small-r expansion of Eq. (A4) which shows

$$E_z(r)\sim E_{\rm tip}, \quad \text{when } r \ll \kappa/2 , \tag{A7}$$

where $\kappa=b^2/a$ and

$$E_z(r)\sim E_0[1+a(a+b)/c^2(a/2r)^{1/2}] , \quad \text{when } a>r>\kappa/2 \tag{A8}$$

$$=E_0[c_{1e}+c_{2e}(a/2r)^{1/2}] , \tag{A9}$$

with

$$c_{1e}=1$$

and (A10)

$$c_{2e}a/(a-b)^{1/2} .$$

Note that c_{1e} and c_{2e} are $O(1)$ as $a\rightarrow\infty$ and $\kappa\rightarrow\infty$.

b. 3D insulating void in a conducting background

The single inclusion shape and orientation that is most effective in enhancing electric fields for this case is penny shaped and oriented perpendicular to the electric field direction. To simulate this we use an oblate ellipsoidal void inclusion, and the electric fields are found by solving the Laplace's equation in ellipsoidal coordinates. The geometry is like that of Fig. 1 of the text, with the ellipsoid found by making a solid of revolution about the z axis. The relationships between Cartesian and oblate ellipsoidal coordinates is given by[10]

$$x=c\cosh\xi\cos\eta\cos\phi ,$$
$$y=c\cosh\xi\cos\eta\sin\phi , \quad \text{(A11)}$$
$$z=c\sinh\xi\sin\eta .$$

The electric potential for a uniform conducting background containing this "penny-shaped" void, with a constant electric field E_0 at infinity in the z direction, is then found by solving Laplace's equation in oblate ellipsoidal coordinates to find

$$\psi_{\text{in}}=-cE_0\sinh\xi\sin\eta[1-(\cot^{-1}\sinh\xi_0-1/\sinh\xi_0)/A] , \quad \text{(A12)}$$

$$\psi_{\text{out}}=-cE_0\sinh\xi\sin\eta[1-(\cot^{-1}\sinh\xi-1/\sinh\xi)/A] , \quad \text{(A13)}$$

where

$$A=\cot^{-1}\sinh\xi_0-\tanh\xi_0/\cosh\xi_0$$
$$=\cot^{-1}(b/c)-bc/a^2 . \quad \text{(A14)}$$

The z-direction electric field as a function of distance, r, from the ellipse tip in $x=y=0$ plane is then given by

$$E_z(\xi)=E_0[1-(\cot^{-1}\sinh\xi-1/\sinh\xi)/A] . \quad \text{(A15)}$$

The electric field at the tip of the defect is found by evaluating Eq. (A15) at $\xi=\xi_0$ and gives

$$E_{\text{tip}}=E_0\{1-[\cot^{-1}(b/c)-(c/b)]/A\} , \quad \text{(A16)}$$

which for large a and small b reduces to

$$E_{\text{tip}}\sim E_0[2/\pi+4a/(\pi b)]$$
$$=E_0[k_{1e}+k_{2e}(a/2\kappa)^{1/2}] \quad \text{(A17)}$$

with

$$k_{1e}=2/\pi$$

and (A18)

$$k_{2e}=4(2^{1/2})/\pi$$

for large a. Rewriting (A15) in terms of the distance from the defect (crack) tip yields

$$E_z(r,z=0)=E_0-E_0\{\cot^{-1}[(a+r)^2/c^2-1]^{1/2}$$
$$-[(a+r)^2/c^2-1]^{-1/2}\}/A , \quad \text{(A19)}$$

and expanding for large r then shows that the "far-field solution" is of a dipole form

$$\sim E_0(1+\alpha_{3e}/r^3) \text{ for } r\gg a , \quad \text{(A20)}$$

where the dipole moment

$$\alpha_{3e}=c^3/3A . \quad \text{(A21)}$$

A small-r expansion of Eq. (A19) shows the near-field solution yields

$$E_z(r)\sim E_0[c_{1e}+c_{2e}(a/2r)^{1/2}] \text{ for } \kappa/2<r<a \quad \text{(A22)}$$

with

$$c_{1e}=2b/\pi c$$

and (A23)

$$c_{2e}=1/A .$$

When $r<\kappa/2$, Eq. (19) reduces to $E_z(r)\sim E_{\text{tip}}$.

2. Dielectric problems

a. 2D problem of a conducting ellipse in an insulating background

The most effective-field enhancing inclusion is a thin ellipse with its long axis parallel to the direction of the electric field (z axis). Mathematically, the solution is identical to that given above for the 2D electrical case (although geometrically the conducting ellipse has its long axis parallel to the applied field), and expression for the electric field at the crack tip, in the near field and in the far field are identical to those given in Eqs. (A5)–(A10) for the electrical case.

b. 3D problem of a conducting ellipsoid in a dielectric background

The most efficient-field enhancing defect is formed by making a solid of revolution about the z axis of an ellipse with its long axis in the z direction. This "fingerlike" inclusion is the most important single inclusion for this dielectric problem. Solving Laplace's equation in the prolate ellipsoidal coordinates[10]

$$x=c\sinh\xi\sin\eta\cos\phi ,$$
$$y=c\sinh\xi\sin\eta\sin\phi , \quad \text{(A24)}$$
$$z=c\cosh\xi\cos\eta$$

leads to the electric potentials

$$\psi_{\text{in}}=0 , \quad \text{(A25)}$$

$$\psi_{\text{out}}=-cE_0\cosh\xi\cos\eta$$
$$\times(1-\{\ln[\tanh(\xi/2)]+1/\cosh\xi\}/B) , \quad \text{(A26)}$$

where

$$B=\ln[\tanh(\xi_0/2)]+1/\cosh\xi_0 . \quad \text{(A27)}$$

The electric field in the z direction at $x=y=0$ as a function of distance from defect tip is then

$$E_z(\xi)=E_0+E_0\{\ln[\tanh(\xi/2)]+\cosh\xi/\sinh^2\xi\}/B . \quad \text{(A28)}$$

From this expression we find the electric field at the defect tip to be

$$E_{\rm tip}=E_0\{1+a^2/[b^2\ln(2a/b)]\} . \quad \text{(A29)}$$

The far-field (large-r) solution again has a dipole form

$$E_z(r)-E_0\sim\alpha_{3d}/r^3 , \quad \text{(A30)}$$

where the 3D electric dipole moment

$$\alpha_{3d}=2c^3/3B . \quad \text{(A31)}$$

For $\kappa<r<a$, the electric field reduces to

$$E_z(r)-E_0=E_0\{[\ln(r/2a)+a/2r]/B\} \quad \text{(A32)}$$

and for $r<\kappa$,

$$E_z(r)\sim E_{\rm tip} . \quad \text{(A33)}$$

3. Elastic problems

a. 2D void in an elastic background

We consider the geometry of Fig. 1 with the external electric field replaced by a tensile stress. The calculation of the stress field due to this inclusion is a standard calculation,[11] and the vertical stress along the horizontal direction is given by [taken from Ref. 11(a), Eq. (130)]

$$\sigma_z(\xi,\eta=0)=\sigma_0(1+\{A[3\exp(-\xi)-\exp(-3\xi)]+B\cosh\xi\}/\sinh^3\xi) , \quad \text{(A34)}$$

where

$$A=\cosh\xi_0[\exp(3\xi_0)-3\exp(\xi_0)] , \quad \text{(A35)}$$

$$B=\cosh^2\xi_0 . \quad \text{(A36)}$$

The stress at the defect tip is then given by

$$\sigma_{\rm tip}=\sigma_0(1+2a/b) . \quad \text{(A37)}$$

Expressing (A34) in terms of r, the radial distance from the crack tip, and doing the large-r expansion, we find

$$\sigma_z(r)-\sigma_0\sim\alpha_{2m}/r^2 \quad \text{for } r\gg a \quad \text{(A38)}$$

with the 2D elastic dipole moment

$$\alpha_{2m}=a^2/2 . \quad \text{(A39)}$$

A small-r expansion of (A34) yields

$$\sigma_z(r)-\sigma_0\sim\sigma_0(a/2r)^{1/2} \quad \text{for } r>\kappa_2=b^2/2a . \quad \text{(A40)}$$

b. 3D void in an elastic background

The most important single defect is a penny-shaped inclusion with its long axis oriented perpendicular to the direction of the applied tensile stress. To study this, we form a solid of revolution about the z axis of the ellipse inclusion of Fig. 1. The exterior stress and strain fields are most easily found using the equivalent inclusion method, and the z-direction stress as a function of distance from the defect tip is given by [this is found after simplifying Eq. (126) of Ref. 11(a)],

$$\sigma_z(\xi)=\sigma_0[1+a^4b(K_1\cot^{-1}\sinh\xi-K_1/\sinh\xi+K_2/\sinh^3\xi)/(c^5N_1)] , \quad \text{(A41)}$$

where

$$K_1=(12-10/\nu)g+2a^4/c^4-(25/22/\nu)a^2c^2 , \quad \text{(A42)}$$

$$K_2=12a^4/c^4-6(g+2)a^2/c^2+6g , \quad \text{(A43)}$$

$$N_1=6[4a^4b^2/c^6-2(1-1/\nu)g^2-(2a^4-8a^2b^2)g/c^4] , \quad \text{(A44)}$$

and

$$g=[a^4b\cot^{-1}(b/c)-a^2b^2c]/c^5 , \quad \text{(A45)}$$

where ν is Poisson's ratio. A plot of (A41) as a function of r (distance from the crack tip) is given in Fig. 2(b). The stress intensity at the defect tip is found to be

$$\sigma_{\rm tip}=\sigma_0\frac{a^2[2a^4/b^4-(1.5-1/\nu)a^2/b^2+1-1/\nu]+a^2A[1/\nu-(1.5+1/\nu)a^2/b^2]}{[(a^2/b^2+1-1/\nu)/bc+a^2A(a^2/b^2-2-2/\nu)-a^4A^2(1+1/\nu)/bc]} , \quad \text{(A46)}$$

where

$$A=\tan^{-1}(c/b) . \quad \text{(A47)}$$

For large a/b and $1/\nu\ll a/b$, we find

$$\sigma_{\rm tip}\sim-\pi(3\nu+2)/4+2a/b=k_{1m}+k_{2m}(a/2\kappa)^{1/2} \quad \text{(A48)}$$

with

$$k_{1m}=-\pi(3\nu+2)/4, \quad k_{2m}=8^{1/2} . \quad \text{(A49)}$$

A large-r expansion, yields the expected dipole behavior

$$\sigma_y(r)-\sigma_0\sim\alpha_{3m}/r^3 \quad \text{for } r\gg a , \quad \text{(A50)}$$

where

$$\alpha_{3m}=(K_2-K_1/3)a^4 b\sigma_0/(c^2N_1) \quad \text{(A51)}$$

is the dipole moment. A small-r expansion yields

$$\sigma_y(r)-\sigma_0\sim 1/r^{1/2} \text{ for small-}r \text{ and } a>r>\kappa/2 \quad \text{(A52)}$$

and

$$\sigma_y(r)\sim\sigma_{\text{tip}} \text{ for } r\ll\kappa/2 \; . \quad \text{(A53)}$$

[1]L. de Arcangelis, S. Redner, and A. Coniglio, Phys. Rev. B **34**, 4656 (1986).

[2]Y. S. Li and P. M. Duxbury, Phys. Rev. B **36**, 5411 (1987); J. Machta and R. A. Guyer, *ibid.* **36**, 2142 (1987); B. Kahng, G. G. Batrouni, and S. Redner, J. Phys. A **20**, L827 (1987); S. K. Chan, J. Machta, and R. A. Guyer, Phys. Rev. B **39**, 9236 (1989); J. Helsing, J. Axell, and G. Grimvall, *ibid.* (to be published).

[3]*Electrical Transport and Optical Properties of Inhomogeneous Media (Ohio State University, 1977),* Proceedings of the First Conference on the Electrical Transport and Optical Properties of Inhomogeneous Media, AIP Conf. Proc. No. **40**, edited by J. C. Garland, and D. B. Tanner (AIP, New York, 1978); D. Stauffer, Phys. Rep. **54**, 1 (1979); see articles in Ann. Israel Phys. Soc. **5** (1983).

[4]Y. Kantor and I. Webman, Phys. Rev. Lett. **52**, 1891 (1984); A. R. Day, R. R. Tremblay, and A. M. S. Tremblay, *ibid.* **56**, 2501 (1986); S. Feng, M. F. Thorpe, and E. Garboczi, Phys. Rev. B **31**, 276 (1985).

[5]P. M. Duxbury, P. D. Beale, and P. L. Leath, Phys. Rev. Lett. **57**, 1052 (1986); P. M. Duxbury, P. L. Leath, and P. D. Beale, Phys. Rev. B **36**, 367 (1987); M. Soderberg, *ibid.* **35**, 352 (1987); B. Kahng, G. G. Bartrouni, S. Redner, L. de Arcangelis, and H. J. Herrmann, *ibid.* **37**, 7625 (1988); P. D. Beale and D. J. Srolovitz, *ibid.* **37**, 5500 (1988); H. J. Herrmann, A. Hansen, and S. Roux, *ibid.* **39**, 637 (1989).

[6]M. A. Dubson, Y. C. Hui, M. B. Weissman, and J. C. Garland, Phys. Rev. B **39**, 6807 (1989).

[7]D. J. Bergman, Phys. Rev. B **39**, 4598 (1989).

[8]See, e.g., R. W. Davidge, *Mechanical Behavior of Ceramics* (Cambridge University Press, Cambridge, England, 1979), Chap. 3.

[9]P. D. Beale and P. M. Duxbury, Phys. Rev. B **37**, 2785 (1988); E. J. Garboczi, *ibid.* **38**, 9005 (1988). Note that the analogy between dielectric breakdown and mechanical fracture drawn in this paper, is only valid in two dimensions. In three dimensions where the most critical defect for the dielectric problem is a fingerlike metal inclusion, while for mechanical problems it is a penny-shaped crack, these problems are very different.

[10]G. Arfken, *Mathematical Methods for Physicists,* 2nd ed. (Academic, New York, 1970).

[11](a) H. Neuber, *Theory of Notch Stresses* (Edwards Brothers, Ann Arbor, Michigan, 1946); (b) Toshio Mura, *Micromechanics of Defects in Solids* (Martinus Nijhoff, Hague, 1982).